Eur. Phys. J. C (2023) 83:1151
https://doi.org/10.1140/epjc/s10052-023-12340-x

THE EUROPEAN PHYSICAL JOURNAL C

Regular Article - Theoretical Physics

Constraining physical parameters of DESs via the secondary component of the GW190814 event and other self-bound NS pulsars in $f(Q)$-gravity theory

Piyali Bhar[1,a], **Abdelghani Errehymy**[2,b], **Saibal Ray**[3,c]

[1] Department of Mathematics, Government General Degree College Singur, Hooghly, West Bengal 712409, India
[2] Astrophysics Research Centre, School of Mathematics, Statistics and Computer Science, University of KwaZulu-Natal, Private Bag X54001, Durban 4000, South Africa
[3] Centre for Cosmology, Astrophysics and Space Science (CCASS), GLA University, Mathura, Uttar Pradesh 281406, India

Received: 12 October 2023 / Accepted: 6 December 2023

Abstract The spherically symmetric dark energy (DE) stellar model is presented here within the context of the $f(Q)$ theory of gravity. In order to develop the model, we take into account the linear functional form of $f(Q)$ as $f(Q) = mQ + n$, where m is the coupling parameter and n is a real constant. We further assume that the stellar model is composed of normal baryonic matter along with DE; however, for the sake of simplicity, we avoid the interaction between them. The impact of the coupling parameter m on different physical parameters of DE stars (DESs) has been thoroughly investigated. For various values of m specified in the figure, the numerical values of the physical parameters are shown in tabular form. It is found that as m increases, the DES candidates become gradually massive and larger in size. In order to compare the behaviour of DESs with the observational results, we use the measurement of the GW190814 event and the three NS pulsars, viz. 4U1608-52 (mass $= 1.74^{+0.14}_{-0.14}\ M_\odot$), PSR J1614-2230 (mass $= 1.97^{+0.04}_{-0.04}\ M_\odot$), and PSR J0952-0607 (mass $= 2.35^{+0.17}_{-0.17}\ M_\odot$). With the help of the $M - R$ plot, the maximum mass of the DES obtained from our model is $2.57\ M_\odot$, which is located within the lower "mass gap" range. To cover the observational constraints, this DES can be a representative for the secondary component of the GW190814 event, whose mass range is detected to be $2.59^{+0.08}_{-0.09}\ M_\odot$ by LIGO/VIRGO experiments.

1 Introduction

The foundation of contemporary astrophysics and cosmology is Einstein's general theory of relativity (GR), which describes gravity as a distortion of spacetime. This hypothesis has some drawbacks, despite precisely describing the effects of gravity on the scale of planets, stars, and the Universe as a whole. Therefore, one must suppose that space is permeated with a mysterious substance known as *DE* whose properties are different from those of any known field, radiation, or particle in order for its predictions to not conflict with observational data on the expansion of the Universe. Numerous studies are being conducted in this area to try and understand the nature of DE.

Therefore, scientists have examined other theories that make predictions that are similar to or identical to those made by Einstein's theory but do not rely on the DE supposition. These theories include $f(R)$, $f(T)$, $f(R,T)$, $f(Q)$ gravity. Recently, specific problems with $f(Q)$ gravity have been considered. Cosmologists now frequently use the $f(Q)$ theory of gravity to explain the acceleration of the Universe in the late universe without resorting to exotic matter distributions. As a step to this issue Bajardi et al. [1] take into account $f(Q)$ extended symmetric teleparallel cosmologies. They are able to minimize and integrate the field equations and thus choose the models that give rise to bouncing cosmology. On the other hand, Mandal et al. [2] examined the cosmological models with the presence of bulk viscosity effect in the cosmological fluid within the framework of $f(Q)$ gravity. A unique model in the context of $f(Q)$ gravity was presented by Anagnostopoulos et al. [3] where a class of gravitational modification solution generated by the inclusion of non-metricity.

[a] e-mail: piyalibhar90@gmail.com
[b] e-mail: abdelghani.errehymy@gmail.com (corresponding author)
[c] e-mail: saibal.ray@gla.ac.in

Published online: 19 December 2023

In order to analyze the accelerated expansion of the universe within the context of modified $f(Q)$ gravity Solanki et al. [4] have looked into the function of bulk viscosity. Interestingly, the bulk viscosity coefficient in the authors' cosmological model, which is dominated by bulk viscous matter, is proportional to the speed and acceleration of the expansion of the universe. Within the framework of symmetric teleparallel gravity $f(Q)$ Sharma et al. [5] examined the solutions of traversable wormholes (WH) with normal matter in the throat. Researchers have attempted to address this problem by utilizing modified gravity theories, where the WH geometry is explained by the extra curvature terms. Thus the null energy conditions are not violated here which indicates the existence of normal matter in the formation of the wormhole geometry. Very recently, Mustafa et al. [6] have studied the wormhole geometry in the galactic halo region under modified $f(Q)$ gravity, especially symmetric teleparallel gravity, where the nonmetricity scalar drives the gravitational interaction. Under a specific functional form of $f(Q)$ two models were presented by them based on the physically motivated shape function and energy conditions to exhibit attributes of the model which are as follows: (i) energy conditions, especially NEC, which is very instructive in connection to energy violation in modified gravity theory, (ii) the wormhole solutions in the regime of Navarro–Frenk–White (NFW) density profiles for the galactic halo regions, (iii) treatment with particles moving in closed orbits around the wormholes which exhibit epicyclic frequencies, and (iv) the red-blue shifts of the light coming from the wormhole throat in the vicinity of the dark matter halos.

By using the gravitational decoupling approach in the context of the vanishing complexity factor condition in $f(Q)$ gravity theory, Jasim et al. [7] examined a spherically symmetric anisotropic solution. The authors used the mimic constraint to density method and the Tolman metric to solve the system of equations. The $f(Q)$ gravity and the minimal geometric deformation (MGD) technique were combined by Maurya et al. [8] to produce compact star (CS) objects with masses aligned with the GW190814 event. They are able to reduce the challenge of completely defining the gravitational behavior of the seed solution to a quadrature by starting with the Tolman IV ansatz for one of the metric functions and an MIT Bag model equation of state. Some more recent works on CS in $f(Q)$ gravity can be found in the following Refs. [9–13]. Some earlier works on compact objects in modified gravity can be found in [14–28].

For spherically symmetric and stationary metric-affine spacetimes that are defined by a metric as well as a flat and torsionless affine connection, DAmbrosio et al. [29] systematically examine the field equations of $f(Q)$ gravity. The reconstruction formalism of the Dirac–Born–Infeld (DBI)-essence scalar field model was studied by Kar et al. [30] in the context of $f(Q)$ gravity, which is governed by the deformation or non-metricity scalar Q and the deformation is pushed about by the fifth dimension of wrapped compact spaces in brane cosmology. In the context of symmetric teleparallelism, Sahoo et al. [31] investigated the periodic cosmic transit behavior of the accelerated universe. Using a well-known deceleration parameter, the field equations have been solved precisely. In $f(Q)$ gravity, where non-metricity Q drives gravitational interactions, Mandal et al. [32] investigated the CSs. The authors take into account a spherically symmetric spacetime with an anisotropic fluid distribution and quintessence field to accomplish this goal. Errehymy et al. [33] studied the characteristics of electrically charged strange stars in $f(Q)$ symmetric teleparallel gravity, whose distribution is governed by the MIT-Bag model equation of state. However, Gadbail et al. [34] established the more general functions of non-metricity scalar Q that admit exact CDM expansion history and offer a variety of exciting explicit reconstructions for the $f(Q)$ gravity in the background of the Friedmann–Laîmatre–Robertson–Walker (FLRW) evolution history. In the framework of $f(Q)$ gravity, Koussour et al. [35] present details of the problems of cosmic acceleration and DE on the basis of homogeneous and isotropic Friedmann–Laîmatre–Robertson–Walker (FLRW) geometry.

In the literature there are a few works available on DESs, e.g. (i) Chapline [36] proposed the DES as a compact object in which the interior region contains much larger vacuum energy that differs from the region from the ordinary spacetime whereas (ii) Lobo [37] studied the stability of a DES by generalizing the concept of gravastar scenario. Very recently Das et al. [38] have proposed a DES under the Einstein-Maxwell field equations with spherically symmetric, charged and anisotropic stellar configuration. However, in the context of DES formations, modified gravity is very much significant. It can enhance the outcomes of modified gravity in comparison to GR without altering the idea of DE. For instance, Tudeshki et al. [39] showed that, in addition to meeting the requirements of DES, the stability of a star close to its surface depends on energy and that the outcomes of gravity's rainbow are superior to those of GR gravity. A model of anisotropic DES has been discussed by Chan et al. [40] which consists of the following four phases: (i) a homogeneous inner core with anisotropic pressure, (ii) an infinitesimal thin shell separating the core and the envelope, (iii) an envelope of inhomogeneous density and isotropic pressure and (iv) an infinitesimal thin shell matching the envelope boundary and the exterior Schwarzschild spacetime. We note an interesting work where Rahaman et al. [41] proposed a singularity-free model of a DES by using the Krori-Barua metric. A wide class of exact interior solutions was established by Yazadjiev [42] representing mixed relativistic stars that contain both ordinary matter and DE in various ratios by adopting the phantom (ghost) scalar field description of DE. On the

other hand, Smerechynskyi et al. [43] investigated the least coupled scalar field DE density distribution inside a neutron star (NS). It is to be noted here that in the hydrodynamical representation, DE is viewed as a perfect fluid with three parameters: the equation of state, the effective sound speed, and the background density.

Astrophysical objects like NS and black hole (BH) mass distributions have been investigated through gravitational-wave (GW) detections of merging NSBH systems, especially in the vicinity of the transition between NS and BH masses. The maximum NS mass, minimum BH mass, and the potential "mass gap" between them are of great interest for this type of merging phenomenon. The detection of GW190814 by the LVC collaboration [44] led to the discovery of a binary system consisting of a 23 $M_\odot$ BH and a CS companion of 2.6 $M_\odot$ (the lower value at 90% credible level being 2.5 $M_\odot$), whereas previous GW population analyses assumed all NSs obey the same maximum mass. However, if rapidly spinning NSs exist, they can extend to larger maximum masses than non-spinning NSs [45]. Since the mass of the companion object falls within the BH lower mass gap, its nature is still undetermined, nevertheless, a massive NS challenges previously imposed astronomical as well as nuclear-physics constraints [46]. Therefore, to resolve the issue it was argued in a recent work by Bombaci et al. [47] that the companion might actually be a Quark Star.

In this regard, we would like to discuss some earlier works also. In a non-minimal geometry matter coupling theory of gravity, Carvalho et al. [48] suggested a model of quark stars. The presented theory can produce a quark star of mass 2.6 $M_\odot$ when $\sigma = 50\, km^2$ a parameter which is appropriate for characterizing the masses of the secondary object in the GW190814 event as well as the pulsars PSR J2215+5135 and PSR J1614-2230. It is noted that even with fast rotation effects, the mass 2.6 $M_\odot$ is such a value that is very difficult to achieve in GR.

In the background of $f(R, T)$ gravity, Deb et al. [49] proposed strange star model by assuming a particular choice of the matter density by taking a linear functional form of $f(R,\ T)$ as $f(R,\ T) = R + 2\xi T$ where ξ is the coupling parameter associated with $f(R,\ T)$ gravity. From their analysis, the authors show that a strange star of mass 3.52 $M_\odot$ can be achieved via the $M - R$ diagram. The authors also examine that the maximum mass and the associated radius decrease with the increasing value of ξ. It can be noted that Tangphati et al. [50] have proposed a strange star described by a color-flavor locked (CFL) model in $f(R, T)$ gravity and find that for CFL EoS supporting $M_{max} > 2.5$ with the radii in the range 10.53–11.39 km. In a very recent study by Tudeshki et al. [51], the maximum mass of a DES in massive gravity goes up to the interval (2.95–3.5) $M_\odot$. In our current paper, we have explored the possibility that such an object could be a DES motivated by the recent identification of compact objects in the (2.5–5.0) $M_\odot$ mass gap [44]. Assuming that the secondary component of the GW190814 event is a CS and not a BH, our analysis focuses on the possibility that CSs have a maximum mass greater than 2.5 $M_\odot$.

With an anisotropic fluid in $f(Q)$ gravity, the present work attempts to investigate possible DESs within the constraints of static and spherically symmetric geometry. Basically, our aim here is to constrain the parameters involved in the model and compare the model parameters with the available data from the observational resources. Keeping this motivation in mind we have structured the article as follows. In Sect. 2, we provide a brief overview of the $f(Q)$ theory which introduces the action and field equations, we discover the DES model for all-purpose static and spherically symmetric geometry and we match the external Schwarzschild line element to our internal spacetime and expressed the metric co-efficient parameter in terms of the mass and radius of the star. In Sect. 3, the physical characteristics of our model are described, especially the mass function, compactness, and surface redshift of our current model are all considered in detail. In Sect. 4, we have demonstrated the stability analysis of our current model. The maximum allowable mass and the corresponding radius along with the measurement of mass with the help of contour plots have been obtained in Sect. 5. Finally, Sect. 6 is devoted to the discussion and conclusion.

2 $f(Q)$ gravity as the background tool for studying compact stellar model

2.1 Field equations for spherically symmetric objects within $f(Q)$ theory

In $f(Q)$ gravity, the action is described by [52]

$$S = \int \left[\frac{1}{2} f(Q) + \mathcal{L}_m\right] \sqrt{-g} d^4x, \tag{1}$$

where g stands for the determinant of the metric $g_{\mu\nu}$, $f(Q)$ represents a general function of Q and $\mathcal{L}_m$ is the matter Lagrangian density.

The expression of the non-metricity tensor $Q_{\alpha\mu\nu}$ is given by

$$Q_{\alpha\mu\nu} = \nabla_\alpha g_{\mu\nu} = -L^\rho_{\alpha\mu} g_{\rho\nu} - L^\rho_{\alpha\nu} g_{\rho\mu}, \tag{2}$$

and it depends on two independent traces given by

$$Q_\alpha = Q_\alpha{}^\beta{}_\beta, \quad \tilde{Q}_\alpha = Q^\beta_{\alpha\beta}. \tag{3}$$

The expression for the deformation term is described by

$$L^\alpha_{\mu\nu} = \frac{1}{2} Q^\alpha_{\mu\nu} - Q^\alpha_{(\mu\nu)}. \tag{4}$$

The definition of the non-metricity scalar is given by

$$Q = -g^{\mu\nu}\left(L^{\alpha}_{\beta\nu}L^{\beta}_{\mu\alpha} - L^{\beta}_{\alpha\beta}L^{\alpha}_{\mu\nu}\right) = -P^{\alpha\beta\gamma}Q_{\alpha\beta\gamma}, \tag{5}$$

where $P^{\alpha\beta\gamma}$ is the non-metricity conjugate and the corresponding tensor is written as

$$P^{\alpha}_{\mu\nu} = \frac{1}{4}\Big[-Q^{\alpha}_{\mu\nu} + 2Q^{\alpha}_{(\mu\nu)} - Q^{\alpha}g_{\mu\nu} - \tilde{Q}^{\alpha}g_{\mu\nu} - \delta^{\alpha}_{(\mu}Q_{\nu)}\Big]. \tag{6}$$

The field equation of $f(Q)$ gravity is obtained by varying (1) with respect to metric coefficients $g_{\mu\nu}$ as

$$-\frac{2}{\sqrt{-g}}\nabla_a\left(\sqrt{-g}f_Q P^{\alpha}_{\mu\nu}\right) + f_Q\left(P^{\alpha\beta}_{\nu}Q_{\mu\alpha\beta} - 2P^{\alpha\beta}_{\mu}Q_{\alpha\beta\nu}\right) + \frac{1}{2}g_{\mu\nu}f = \kappa T_{\mu\nu}, \tag{7}$$

where $f_Q = \frac{\partial f}{\partial Q}$ and the energy-momentum tensor $T_{\mu\nu}$ is given by

$$T_{\mu\nu} = -\frac{2}{\sqrt{-g}}\frac{\delta\sqrt{-g}\mathcal{L}_m}{\delta\sqrt{g_{\mu\nu}}}. \tag{8}$$

The following equation can be obtained by varying the action with regard to the affine connection

$$\nabla_{\mu}\nabla_{\nu}\left(\sqrt{-g}f_Q P^{\mu\nu}_{\alpha}\right) = 0. \tag{9}$$

The field equations ensure the conservation of the energy–momentum tensor within the framework of $f(Q)$ gravity and the Einstein field equations are restored for the choice of $f(Q) = Q$.

Let us assume that the interior spacetime of the spherically symmetric static stellar configuration in curvature coordinates $(t,\ r,\ \theta,\ \phi)$, is described by the following line element:

$$ds^2_{-} = e^{\nu}dt^2 - e^{\lambda}dr^2 - r^2(d\theta^2 + \sin^2\theta d\phi^2), \tag{10}$$

where λ and ν are functions of r. If both the metric coefficients $\nu(r)$ and $\lambda(r)$ tend to zero as r approaches to ∞, the spacetime will be asymptotically flat. The metric coefficients play an important role in calculating the mass and redshift functions of the stellar model.

The expression of the non-metricity scalar in terms of the metric coefficients is described by [53]

$$Q = \frac{1}{r}(\nu' + \lambda')(e^{-\lambda} - 1). \tag{11}$$

Let us assume that our proposed stellar structure is made of normal baryonic matter along with DE and for the sake of simplicity it is assumed that there is no interaction between them. Two fluid systems in the astrophysical realm are not unavailable as far as the literature survey is concerned. In their work Rahaman et al. [54] besides 'the real matter source an anisotropic DE' also have considered. Kuhfittig [55] have successfully studied 'two noninteracting fluids beginning with a combined model of ordinary matter and phantom DE with an anisotropic matter distribution'. In actual situation, in any two-fluids system there might have internal interactions which is even now not known distinctively due to lack of the proper equation of state. So, customarily those are treated as non-interactive to avoid complexity in the interior of the system.

Therefore, the energy-momentum tensor is thought to be made up of both ordinary matter along with DE. We also assume that the ordinary matter has a density ρ and pressure p. In addition, the DE component has radial pressure of p_r^D, and a tangential pressure of p_t^D, and the DE has a density of ρ^D, as well. The expression of the energy-momentum tensor is given by [56]

$$T^0_0 = \rho + \rho^D, \tag{12}$$
$$T^1_1 = -(p + p_r^D), \tag{13}$$
$$T^2_2 = T^3_3 = -(p + p_t^D), \tag{14}$$
$$T^1_0 = T^0_1 = 0. \tag{15}$$

The DE density can be represented in terms of the (variable) cosmological constant Λ as $\rho^D = \frac{\Lambda c^2}{8\pi G}$ [56]. Hence, the field equations for DES in $f(Q)$ gravity are given by [75]

$$\rho + \rho^D = \frac{e^{-\lambda}}{2\kappa r^2}\Big[2rf_{QQ}Q'(e^{\lambda} - 1) + f_Q\Big((e^{\lambda} - 1)(2 + r\nu') + (1 + e^{\lambda})r\lambda'\Big) + fr^2e^{\lambda}\Big], \tag{16}$$

$$p + p_r^D = -\frac{e^{-\lambda}}{2\kappa r^2}\Big[2rf_{QQ}Q'(e^{\lambda} - 1) + f_Q\Big((e^{\lambda} - 1) \times (2 + r\lambda' + r\nu') - 2r\nu'\Big) + fr^2e^{\lambda}\Big], \tag{17}$$

$$p + p_t^D = -\frac{e^{-\lambda}}{4\kappa r}\Big[-2rf_{QQ}Q'\nu' + f_Q\Big(2\nu'(e^{\lambda} - 2) - r\nu'^2 + \lambda'(2e^{\lambda} + r\nu') - 2r\nu''\Big) + 2fre^{\lambda}\Big], \tag{18}$$

where $\kappa = 8\pi$ and prime denotes the derivative with respect to the radial coordinate r.

The following equation can be used to represent the conservation equation referred to as the TOV equation, for the anisotropic fluid:

$$-\frac{d}{dr}(p + p_r^D) - \frac{\nu'}{2}\left(\rho + \rho^D + p + p_r^D\right) + \frac{2}{r}\left(p_t^D - p_r^D\right) = 0. \tag{19}$$

2.2 Modelling DES within $f(Q)$ theory

To solve the above field equations, let us assume the following metric coefficients:

$$\lambda = ar^2,\ \nu = br^2 + d, \tag{20}$$

proposed by Krori and Barua [57]. Henceforth this metric potential will be termed as KB metric which has been utilized by several scientists (i) to study CSs, especially interior astrophysics of NSs, and (ii) by including it to generate a singularity free solutions [58–68]. Here both a and b are numeric constants having unit km^{-2} and d is a dimensionless quantity. However. it is to be noted that suitable boundary conditions can be used to identify the values of the three unknown constants present in the *ansatz*.

We assume the simplified and linear functional form of $f(Q)$ as follows:

$$f(Q) = mQ + n, \tag{21}$$

where m is the coupling parameter and n is a numerical constant.

With the help of the Eqs. (20)–(21), the field equations (16)–(18) take the following form:

$$\kappa(\rho + \rho^D) = \frac{n}{2} + \frac{e^{-ar^2}m(-1 + e^{ar^2} + 2ar^2)}{r^2}, \tag{22}$$

$$\kappa(p + p_r^D) = -\frac{n}{2} + \frac{m\left\{-1 + e^{-ar^2}(1 + 2br^2)\right\}}{r^2}, \tag{23}$$

$$\kappa(p + p_t^D) = -\frac{n}{2} - (a - b)e^{-ar^2}m(1 + br^2). \tag{24}$$

Now we are in a position to solve Eqs. (22)–(24). Inspired by the works of several authors given in the following Refs. [41,56,79], let us assume that the radial pressure associated with DE (p_r^D) is proportional to the DE density, i.e.,

$$p_r^D = -\rho^D. \tag{25}$$

At the same time, it is also assumed that the density corresponding to DE is proportional to the normal baryonic matter density, i.e.,

$$\rho^D = \alpha\rho, \tag{26}$$

where α is a non-negative constant for certain obvious physical causes [56] and it will be calculated from the boundary conditions.

We obtain the matter density and the pressure for the normal baryonic matter by solving the field equations (22)–(24) with the help of (25) and (26) as follows:

$$\rho = \frac{nr^2 + 2m\left\{1 + e^{-ar^2}(-1 + 2ar^2)\right\}}{2(1 + \alpha)\kappa r^2}, \tag{27}$$

$$p = \frac{e^{-ar^2}\left\{2m + 4\big(b + \alpha(a + b)\big)mr^2 - e^{ar^2}(2m + nr^2)\right\}}{2(1 + \alpha)\kappa r^2}. \tag{28}$$

Now we are interested in finding out a relationship between the ordinary matter density ρ and the corresponding pressure p. Now using the Eqs. (27)–(28) and doing some mathematical calculations and taking the first two terms of the series expansion of e^{ar^2}, and e^{-ar^2} we finally arrived at the following equation.

$$\begin{aligned} p = {} & \frac{1}{72a^2\kappa(1 + \alpha)m^2}\Big[\big\{n - 2(1 + \alpha)\kappa\rho\big\} \\ & \times\big\{12a^2(1 - 2\alpha)m^2\big\} \\ & + \Big\{12am\big(-2(1 + \alpha)bm + n\big) \\ & + n\big(n - 2(1 + \alpha)\kappa\rho\big)\Big\}\Big] \end{aligned} \tag{29}$$

From the above equation we can see that pressure follows a nonlinear relationship with density.

The matter density, and radial and transverse pressures due to the DE are obtained as

$$\rho^D = \frac{\alpha\left\{nr^2 + 2m\left(1 + e^{-ar^2}(-1 + 2ar^2)\right)\right\}}{2(1 + \alpha)\kappa r^2}, \tag{30}$$

$$p_r^D = -\frac{\alpha\left\{nr^2 + 2m\left(1 + e^{-ar^2}(-1 + 2ar^2)\right)\right\}}{2(1 + \alpha)\kappa r^2}, \tag{31}$$

$$\begin{aligned} p_t^D = {} & \frac{e^{-ar^2}}{2(1+\alpha)\kappa r^2}\big\{e^{ar^2}(2m - \alpha nr^2) + (1+\alpha)(a-b)br^4 \\ & - 2m\left(1 + (a + 3a\alpha + b + \alpha b)r^2\right)\big\}. \end{aligned} \tag{32}$$

In the next sections, we shall examine the physical viability of our current model.

2.3 Exterior spacetime in the case of $f(Q)$ gravity

To determine the values of four unknown constants, we have to smoothly match our interior spacetime to the exterior Schwarzschild [69] line element at the boundary $r = R$. The exterior spacetime is as follows:

$$\begin{aligned} ds_+^2 = {} & \left(1 - \frac{2m(r)}{r}\right)dt^2 - \left(1 - \frac{2m(r)}{r}\right)^{-1}dr^2 \\ & - r^2(d\theta^2 + \sin^2\theta d\phi^2), \end{aligned} \tag{33}$$

corresponding to the interior line element given in (10).

The continuity of metric potential and its derivative over the boundary Σ thus constitute the first fundamental form. Which explicitly gives

$$\frac{1}{1 - \frac{2M}{R}} = e^{aR^2}, \tag{34}$$

$$1-2\frac{M}{R}=e^{bR^2+d}, \tag{35}$$

$$\frac{M}{R^3}=be^{bR^2+d} \tag{36}$$

where $M=m(r)|_{r=R}$ being the mass of the CS.

The continuity of extrinsic curvature across the boundary yields $p_r(R)=0$ which gives

$$\alpha=-\frac{2m-2e^{aR^2}m+4bmR^2-e^{aR^2}nR^2}{4(a+b)mR^2}. \tag{37}$$

Equations (34)–(36) are solved to obtain the following expressions for the model parameters:

$$b=\frac{M}{R^3}\left(1-2\frac{M}{R}\right)^{-1},$$

$$d=\ln\left[1-2\frac{M}{R}\right]-\frac{M}{R}\left(1-2\frac{M}{R}\right)^{-1},$$

$$a=-\frac{1}{R^2}\ln\left[1-2\frac{M}{R}\right].$$

3 Physical attributes of the present model on dark star

To ensure that the model is able to precisely explain the stellar structure of anisotropic DESs, we study the structural physical parameter behavior of the anisotropic DES model and the model parameters depending on the physical conditions.

3.1 Regularity of metric coefficient

Singularities are acknowledged as a major problem in the study of relativistic DESs. Therefore, we study the nature of the metric coefficients at the core of these stars. The metric coefficients in DESs must be regular and positive for the solutions to be physically tractable [70]. From Eq. (20), we can see that

$$\frac{d}{dr}\left[e^{\nu}\right]=2bre^{br^2+d},\ \frac{d^2}{dr^2}\left[e^{\nu}\right]=\left(1+2br^2\right)e^{br^2+d}. \tag{38}$$

This gives $\frac{d}{dr}\left[e^{\nu}\right]_{r=0}=0$ and $\frac{d^2}{dr^2}\left[e^{\nu}\right]_{r=0}>0$ at the stellar core. We can also notice in Eq. (20) that the other metric co-efficient ensures the form $\left[e^{\lambda}\right]_{r\neq 0}=1+O(r^2)$ near the stellar core. Therefore, the metric coefficients considered are regular, well-behaved, and free from central singularity throughout the stellar interior. Figure 1 shows the nature of the metric coefficients for our present model.

3.2 Nature of pressure and density

The equilibrium gravitational mass that can be obtained at a stable stellar radius is strongly influenced by the stellar energy density, which plays a critical role in its measurement.

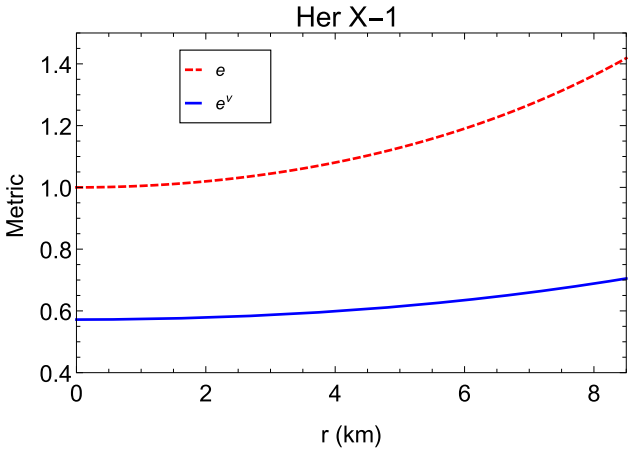

Fig. 1 Metric coefficients are shown against 'r'

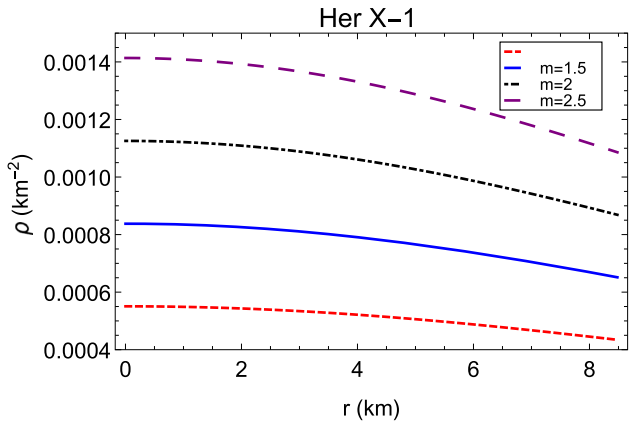

Fig. 2 Density functions are shown against 'r'

For gravitationally confined DESs, the stellar energy density is expected to be maximum at the core and gradually decrease towards the surface. The behavior of the matter density, $\rho(r)$, has been shown in Fig. 2. It is interesting to observe that the matter density is largest at the center and monotonously reduces with increasing stellar radius, r, reaching a minimum at the stellar surface for every branch of the parameter, $m\in[1.0,\ 2.5]$. The central matter density of our current model can be obtained as follows:

$$\rho_c=\rho|_{r=0}=\frac{6am+n}{2\kappa+2\alpha\kappa}\geq 0. \tag{39}$$

We obtained that the maximum of the stellar density lies in the range, $\rho_c\in[0.00014,\ 0.00055]\ \mathrm{km}^{-2}$ at the center, $r=0$ and at the stellar surface, $r=R$, the surface density lies in the range, $\rho_s\in[0.00011,\ 0.00040]\ \mathrm{km}^{-2}$. It should be noted that the parameter m favors gravitational condensation of matter at lower densities, as increasing m causes $\rho(r)$ to shift to lower equilibrium values everywhere in the stellar interior, $r<R$.

For CSs, the inner pressures should be maximal and finite at the center and, more precisely, the radial component should

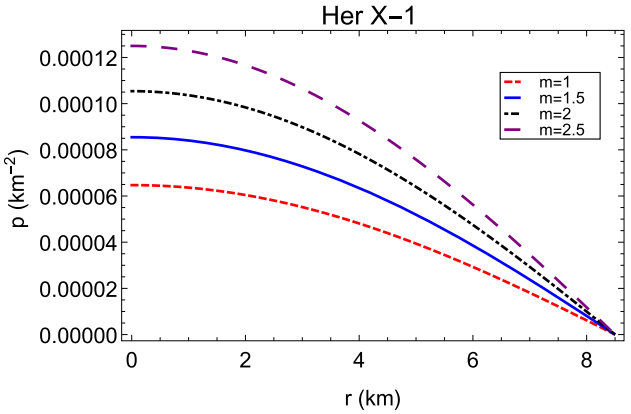

Fig. 3 Pressures are shown against 'r'

disappear at the surface. The behavior of this pressure has been shown in Fig. 3. It is interesting to note that for each branch of the parameter, $m \in [1.0,\ 2.5]$, the pressure remains finite everywhere in the stellar interior with the largest values at the center and the lowest values at the stellar surface. The obtained expression for this pressure at the center turns out to be

$$p_c = p|_{r=0} = \frac{2a(-1+2\alpha)m + 4(1+\alpha)bm - n}{2(1+\alpha)\kappa} \geq 0. \tag{40}$$

On the other side, Fig. 4 shows the density and pressure profiles brought on by DE. It is interesting to note that all three quantities, namely the DE density ρ^D, radial and transverse pressures brought on by DE p_r^D and p_t^D, respectively, are monotonically decreasing functions with increasing stellar radius, r. The DE density is positive whereas the radial and transverse pressures consistent with DE are negative in our present model.

According to Zeldóvich and Novikov [74], the relationship between the central pressure and the central density, viz., $\rho_c - p_c \geq 0$ for a stable stellar structure must be satisfied. From this relationship, we can obtain the Zeldóvich ratio which is as follows:

$$\frac{p_c}{\rho_c} \leq 1 \Rightarrow -1 + \frac{4(1+\alpha)(a+b)m}{6am+n} \leq 1, \tag{41}$$

which implies that this ratio must be less than unity.

Combining the inequalities in (40) and (41), we get the following bound for α as

$$\frac{n+2a-4bm}{4(a+b)m} \leq \alpha \leq \frac{2am+n-4bm}{4(a+b)m}. \tag{42}$$

Let us propose a new parameter, ω, defined by, $\omega = \frac{p}{\rho}$ to discuss the composition of the underlying fluid inside the stellar structure whose expression is given by

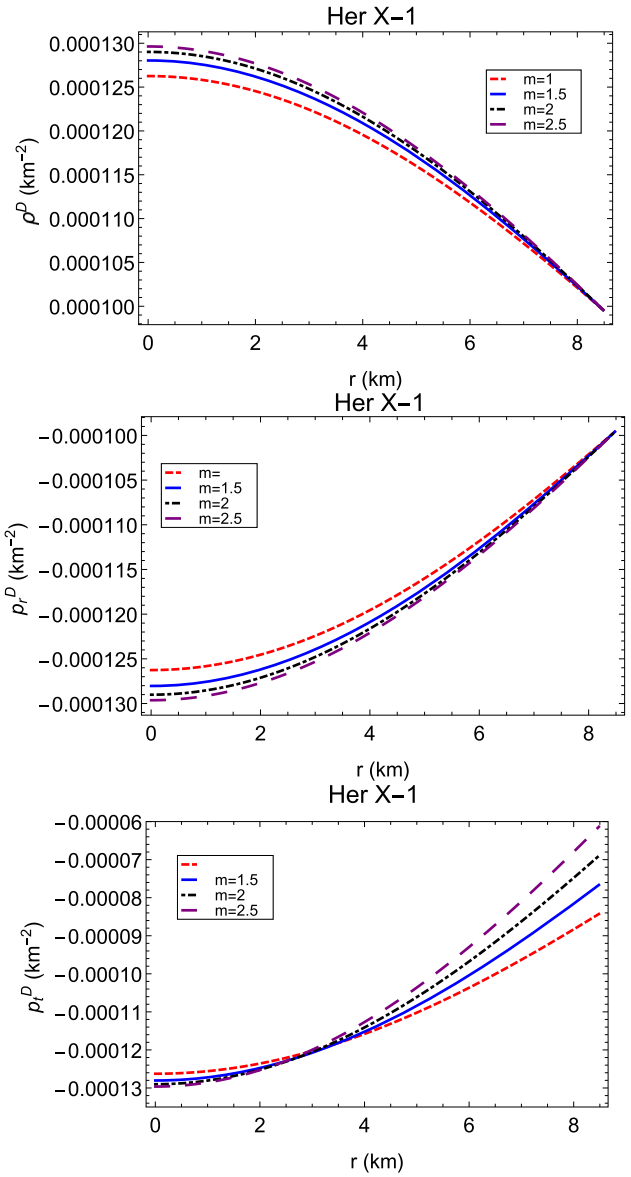

Fig. 4 ρ^D, p_r^D, p_t^D are shown against 'r'

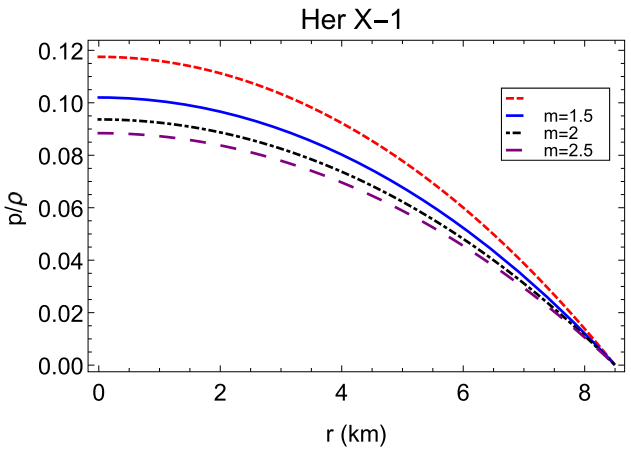

Fig. 5 The equation of state $\omega = \frac{p}{\rho}$ are shown against 'r'

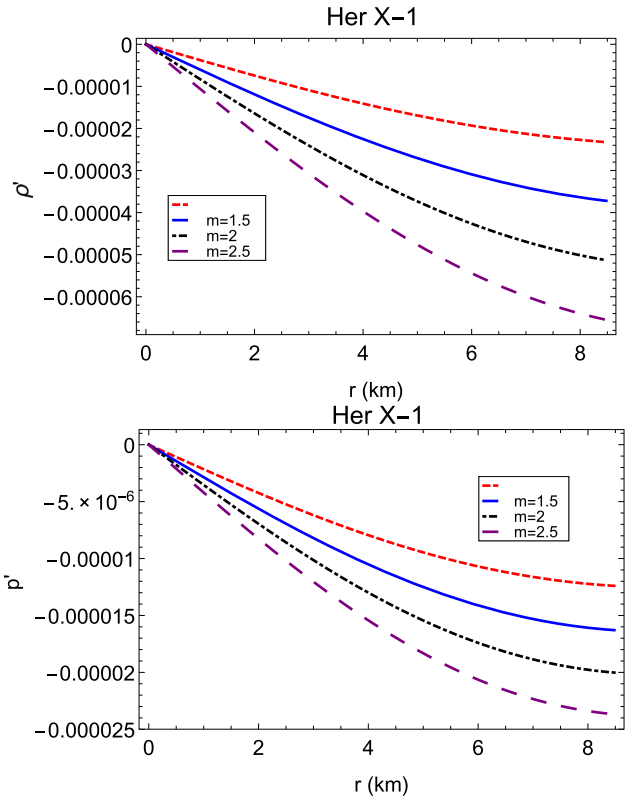

Fig. 6 The density and pressure gradients are shown against 'r'

$$\omega(r) = \frac{p}{\rho} = \frac{4(1+\alpha)(a+b)mr^2}{2m(-1+2ar^2)+e^{ar^2}(2m+nr^2)} - 1, \tag{43}$$

Figure 5 clearly shows that our model star, Her X-1, fulfills the Zeldóvich ratio as $\omega(r) = \frac{p}{\rho}$ for all causal branches of the parameter, $m \in [1.0,\ 2.5]$ everywhere in the stellar interior.

The density and pressure gradients for our present model are obtained as follows:

$$\rho' = -\frac{2e^{-ar^2}m\left\{e^{ar^2}+(-1+ar^2)(1+2ar^2)\right\}}{(1+\alpha)\kappa r^3} \tag{44}$$

$$p' = \frac{2e^{-ar^2}m\left\{-1+e^{ar^2}-ar^2-2a\big(b+\alpha(a+b)\big)r^4\right\}}{(1+\alpha)\kappa r^3}. \tag{45}$$

These gradients are expected to be negative within the compact stellar systems; their actual effect in this study is displayed in Fig. 6. As shown in this graph, we have come to the conclusion that all derivatives of density and pressure are negative and have decreasing trends. The negative nature of these gradients demonstrates the physical comfort of our solutions, which are thought to be necessary for astrophysical modeling.

3.3 Energy conditions for the system

It is well-known that energy conditions play a crucial role in explaining the existence of compact stellar structures. These energy conditions are divided into four categories: null energy, weak energy, strong energy, and dominant energy conditions, which are progressively symbolized by E_{null}, E_{weak}, E_{strong} and E_{dominant} which are defined as

$$E_{\text{null}}:\ \rho+p\geq 0,\ E_{\text{weak}}:\ \rho+p\geq 0,\ \rho\geq 0,$$
$$E_{\text{strong}}:\ \rho+p\geq 0, \rho+3p\geq 0,\ E_{\text{dominant}}:\ \rho-p\geq 0,$$
$$\rho\geq 0.$$

From the above definitions of different energy conditions, one can easily note that it is necessary to use the following expressions to check the energy conditions:

$$\rho+p = \frac{2(a+b)e^{-ar^2}m}{\kappa}, \tag{46}$$

$$\rho-p = \frac{e^{-ar^2}}{(1+\alpha)\kappa r^2}\Big\{-2m-2\big(a(-1+\alpha)+b+\alpha b\big)mr^2 + e^{ar^2}(2m+nr^2)\Big\}, \tag{47}$$

$$\rho+3p = \frac{e^{-ar^2}}{(1+\alpha)\kappa r^2}\Big\{2m\big(1+(a+3a\alpha+3(1+\alpha)b)r^2\big) - e^{ar^2}(2m+nr^2)\Big\}. \tag{48}$$

Figure 7 clearly shows that all energy conditions, viz., E_{null}, E_{weak}, E_{strong} and E_{dominant} are fulfilled throughout the stellar interior, for the considered $f(Q)$ model.

3.4 Mass–radius relationship

By resolving the differential equation

$$\frac{dm(r)}{dr} = 4\pi\rho(r)r^2 \tag{49}$$

and using the initial boundary condition $m(0) = 0$ [94], we were able to derive the mass function for the current stellar model. From the solution relates, the mass function $m(r)$ turns out to be

$$m(r) = 4\pi\int_0^r \rho(r)r^2dr = \frac{6\left(1-e^{-ar^2}\right)mr+nr^3}{12(1+\alpha)}, \tag{50}$$

where one can note that for the definition of the mass we have taken the physical system to be spherically symmetric as per the prescription suggested by several investigators [78, 87, 110].

The redshift $z_s(r)$ can be obtained as

$$z_s(r) = \left(1-2\frac{m(r)}{r}\right)^{-\frac{1}{2}} - 1. \tag{51}$$

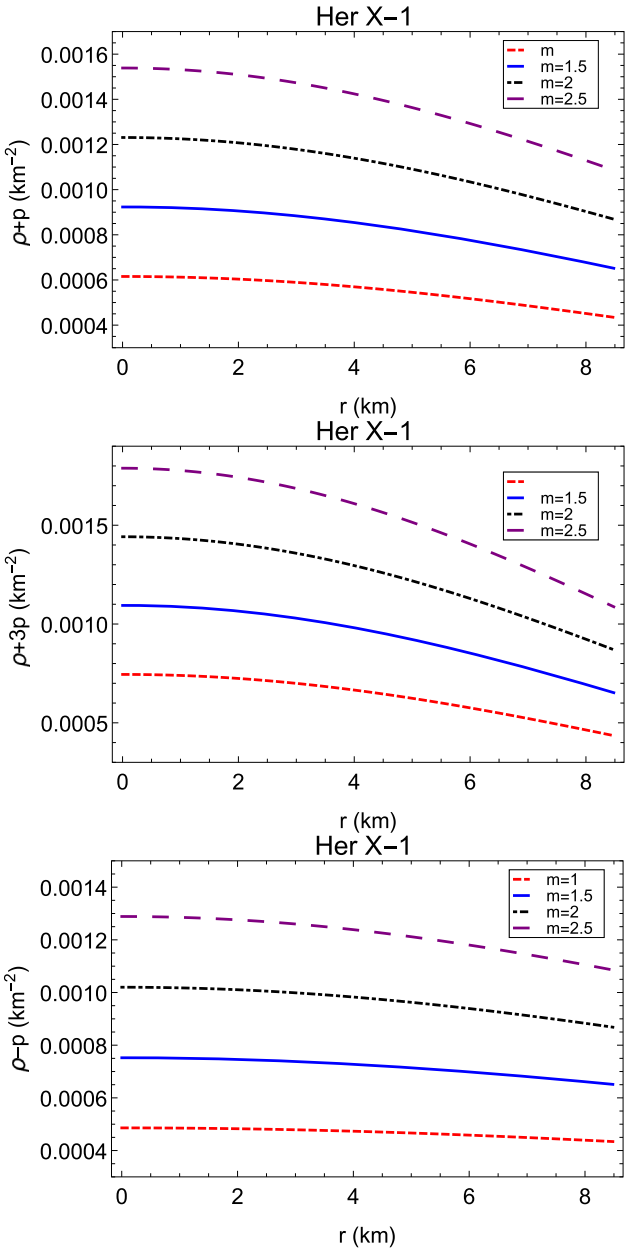

Fig. 7 The energy conditions are shown against 'r'

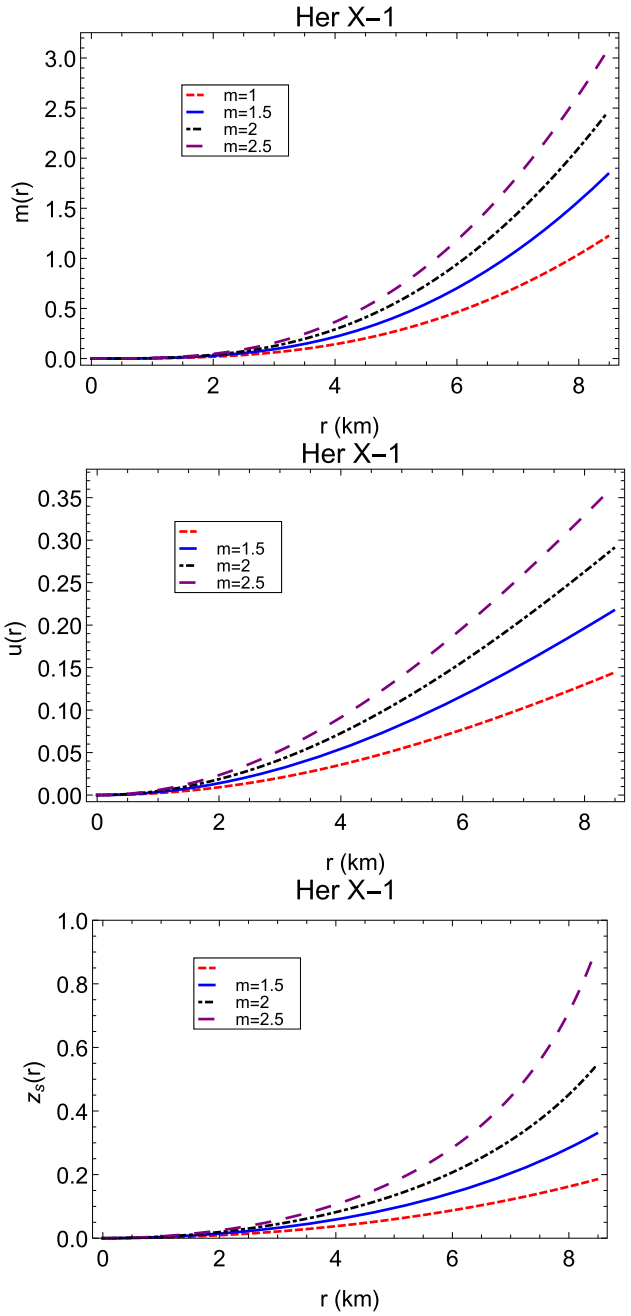

Fig. 8 The mass function, compactness factor, and surface redshift are shown against 'r'

From the expression of $z_s(r)$, one can easily check that $z_s(r)$ depends on a term $\frac{m(r)}{r}$ which is called the compactness factor and it is denoted by $u(r)$.

Figure 8 shows how the mass function $m(r)$, compactness factor $u(r)$, and surface redshift $z_s(r)$, vary in relation to the radial coordinate, r. The graphic demonstrates that each physically significant variable satisfies the criteria of an attainable celestial configuration. It should be noted that the mass function at the center is guaranteed to be regular and that it reaches its highest value at the stellar surface. Additionally, the three quantities are positive inside the stellar body and have monotonic growing functions against the radius r. On the other hand, the surface redshift is satisfied throughout the stellar structure, based on the constraints imposed by scientists [85,98] that the surface redshift of an anisotropic fluid sphere must be less than $z_s \leq 5$ or $z_s \leq 5.211$, which proves that our stellar model is acceptable.

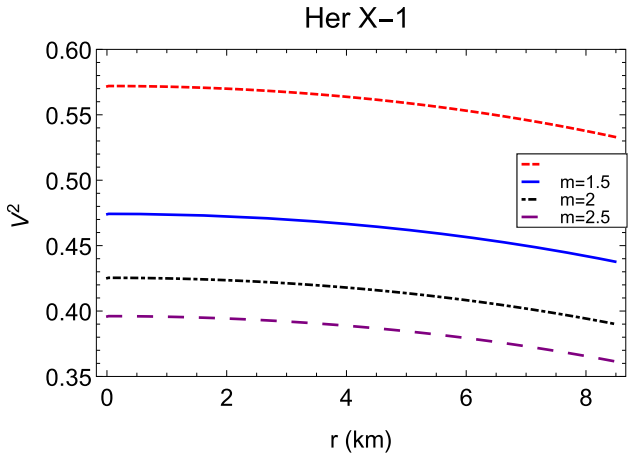

Fig. 9 The square of sound velocities are shown against 'r'

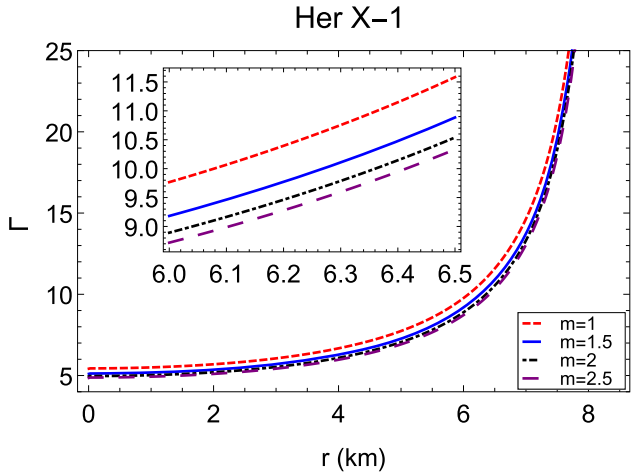

Fig. 10 The relativistic adiabatic indices are shown against 'r'

4 Stability analysis of the spherical configuration

4.1 Causal conditions

For a physically valid and hence agreeable stellar model, the ultra-relativistic velocity of sound must be less than the velocity of light, i.e., remain causal: $V^2 < 1$ everywhere in the stellar interior in order to satisfy the causality condition. The expression for the velocity of sound, V^2 in our current model can be obtained as

$$V^2 = \frac{dp}{d\rho} = \frac{1 - e^{ar^2} + ar^2 + 2a\big(b + \alpha(a+b)\big)r^4}{e^{ar^2} + (-1 + ar^2)(1 + 2ar^2)}. \tag{52}$$

As can be seen in Fig. 9, we find that the ultra-relativistic velocity of sound V^2 satisfies the necessary causality condition throughout the stellar interior, for different values of the parameter, m located in the interval $(1,\ 2.5)$. It is also noticeable that the ultra-relativistic velocity of sound V^2 decreases with a maximum value at the center when the contribution of DE increases. This phenomenon can be explained by a general drop in the stable stellar density of the model star as the parameter (m) grows.

4.2 Dynamical stability

The adiabatic index can be employed to describe the rigidity of the equation of state for a given specific energy density, which confirms the stability of stellar structures both relativist and non-relativistically. The notion of dynamical stability for infinitesimal radial adiabatic oscillations of stellar spheres was originally developed by Chandrasekhar [88]. Several researchers have tested this notion of dynamical stability for both isotropic and anisotropic stellar configurations [86,91,95–97,109]. For compact stellar models to be stable, the value of the adiabatic index, Γ must be greater than $4/3$.

This adiabatic index, Γ can be expressed as

$$\Gamma = \frac{\rho + p}{p} V^2, \\ = \frac{4(1+\alpha)(a+b)mr^2}{2m + 4\big(b + \alpha(a+b)\big)mr^2 - e^{ar^2}(2m + nr^2)} V^2. \tag{53}$$

From Fig. 10, it can be stated that the $f(Q)$ model under consideration could be balanced under the above stability condition. Interestingly, the adiabatic index Γ drops as the parameter m grows, indicating that DE reduces the degree of rigidity of the underlying equation of state for the astrophysical model.

4.3 TOV equation

In this subsection, we are going to verify the equilibrium of our present model under different forces. The Eq. (19) can be written as,

$$F_g + F_h + F_d = 0, \tag{54}$$

where, $F_g = -\frac{\nu'}{2}(\rho + p)$, $F_h = -\frac{dp}{dr}$, $F_d = -\frac{\nu'}{2}(\rho^D + p_r^D) + \frac{2}{r}(p_t^D - p_r^D)$.

Here F_g is called the gravitational force, F_h is the hydrostatics force and F_d is the force related to the dark energy.

The nature of all three forces is shown in Fig. 11 for different values of 'm'. From the figures, one can note that both F_g and F_d are repulsive in nature and their combined effects are balanced by F_h to keep the model in equilibrium.

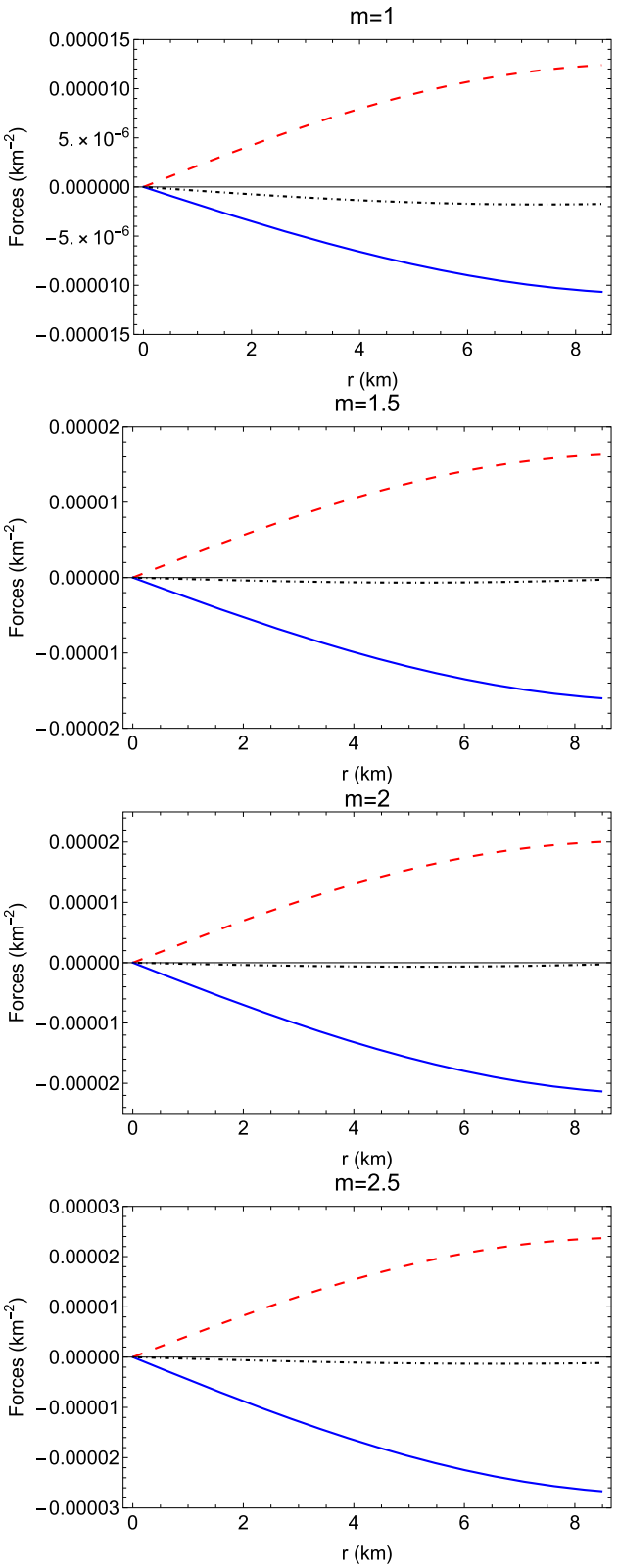

Fig. 11 Different forces acting on the model. Here red long dashed line, black dot-dashed line, and blue solid line respectively denotes the forces F_h, F_d and F_g

5 Constraining physical parameter: maximum allowable mass

In order to compare the behavior of a DES in the context of $f(Q)$ gravity with the observational results obtained so far, in the present work, we use the observational measurement of the GW190814 event and the 3 NS pulsars. In Fig. 12 we have drawn four horizontal stripes of different colors representing the mass range of four different NSs, viz. 4U1608-52, PSR J1614-2230, PSR J0952-0607 and GW190814 with their associated masses respectively as $1.74^{+0.14}_{-0.14}\ M_\odot$, $1.97^{+0.04}_{-0.04}\ M_\odot$, $2.35^{+0.17}_{-0.17}\ M_\odot$ and $2.59^{+0.08}_{-0.09}\ M_\odot$. In Fig. 12, for the chosen values of $m = 1$, 1.5, 2, and 2.5 we have plotted the total mass M (normalized in $M_\odot$) versus the radius R for the DES candidates. The figure indicates that the maximum value of mass (M_{max}) gradually increases for the increasing values of m. For our present model, the maximum allowable mass and the corresponding radius for different values of m are presented in Table 3. For our present model, the maximum masses are ranges in 1.71 $M_\odot$–2.57 $M_\odot$. The radii corresponding to the maximum masses lie in 7.7–9.06 km. From our analysis, we have shown that the masses of the four NSs mentioned above can be achieved by our proposed model of DESs for different chosen values of m.

In this connection, we want to mention that the secondary mass of GW190814 lies in the hypothesized lower "mass gap" of (2.5–5) $M_\odot$ between known NSs and BHs [82,92,100,101]. It is heavier than the most massive pulsar in the Galaxy [89], and almost exceeds the mass of the (1.61–2.52) $M_\odot$ primary component of GW190425, which is itself an outlier relative to the Galactic population of BNSs [80]. It is also comparable to the millisecond pulsar PSR J1748-2021B [93] whose mass is claimed $2.74^{+0.21}_{-0.21}\ M_\odot$ at 68% confidence. An important observation in this paper is that in the context of $f(Q)$ gravity, for $m = 2.5$ we achieved a DES of mass 2.57 $M_\odot$ lies in the hypothesized lower "mass gap". Our result is also compatible with the new data for PSR J0952-0607 (mass = $2.35^{+0.17}_{-0.17}\ M_\odot$), the heaviest and fastest pulsar in the disk of the Milky Way which supports the possible existence of strange quark matter in its composition. This pulsar is a 707 Hz binary millisecond pulsar which was found by using LOFAR at a central observing frequency of 135 MHz, well below the 300 MHz to 3 GHz frequencies typically used in pulsar searches. It was initially reported by Bassa et al. [83]. It is a "black widow binary" with a low-mass (sub-stellar) companion being irradiated and evaporated by the pulsar's luminosity. In the work of Astashenok et al. [84], the R^2 model scenario shows that the $\sim 3M_\odot$ general relativistic limit is respected because the upper causal mass limit is marginally equal to the general relativistic causal maximum mass and is within, but not deeply in, the mass-gap zone. The authors also discuss the strange star hypothesis in light

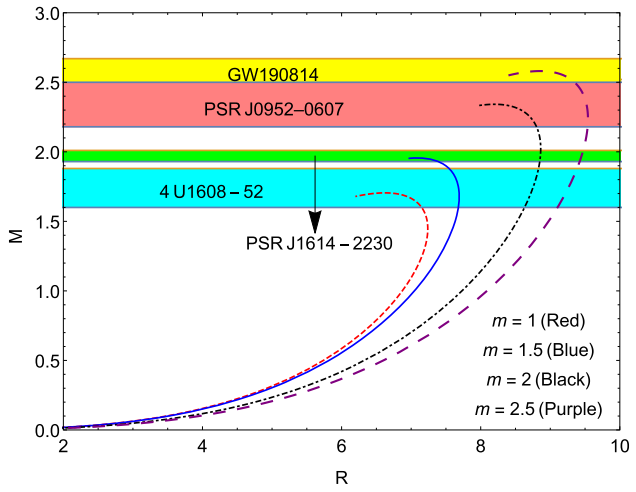

Fig. 12 M–R relationship

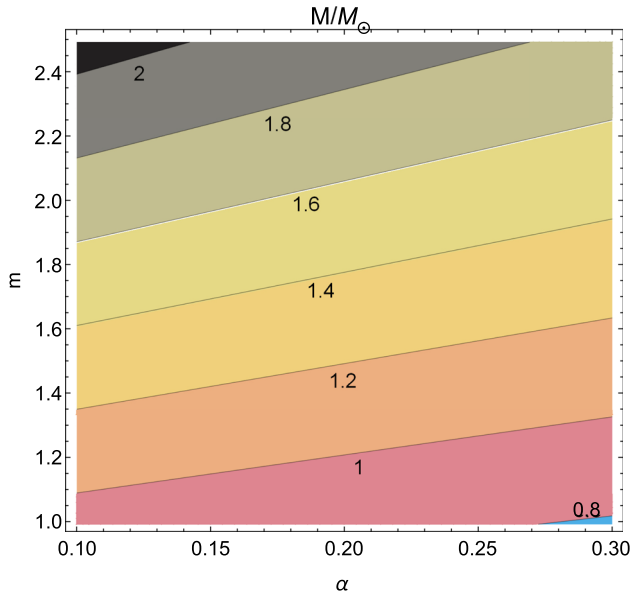

Fig. 13 Contour plot of the mass M($M_\odot$) on $\alpha - m$ plane with $n = 0.005$

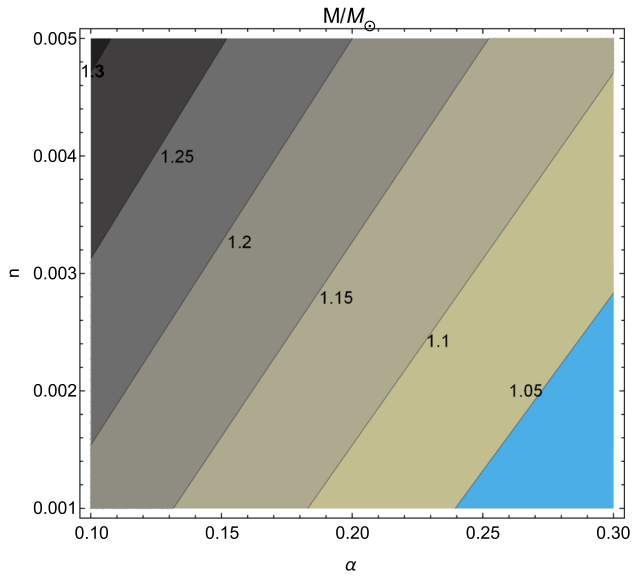

Fig. 14 Contour plot of the mass M($M_\odot$) on $\alpha - n$ plane with $m = 1.5$

of the modified gravity perspective for the secondary component of the GW190814 event. Odintsov and Oikonomou [28] studied the static neutron stars in the context of several inflationary models that are popular in cosmology. By using MPA1 equation of state, the authors showed that the maximum masses of the neutron stars are in the mass-gap region with $M > 2.5\ M_\odot$, but lower than the three solar masses causal limit.

5.1 Measuring of mass

5.1.1 Through equi-mass profiles

By fixing $n = 0.005$ and $r = 8.5$, the equi-mass diagram on the $\alpha - m$ plane is displayed in Fig. 13. The figure shows that, when α is fixed, mass increases with an increasing value of m. On the other hand, assuming a fixed value of m, the mass decreases as α increases.

Again, by fixing m at 1.5 and $r = 8.5$, the equi-mass diagram on the $\alpha - n$ plane is shown in Fig. 14. It is evident from the diagram that, given a fixed value of α, the mass increases as n increases. On the other hand, when n is fixed, the mass decreases as α increases.

To demonstrate the nature of the equi-mass diagram in the $m - n$ plane, we draw Fig. 15 by fixing α and r at 0.25 and 8.5, respectively. The figure shows that the mass increases with an increasing value of n for a fixed value of m. When n is fixed, the mass also increases for increasing values of m.

5.1.2 Through $M - \rho_c$ curve

We have shown the variation of mass (M in the top panel) and radius (R in the bottom panel) with respect to central density ρ_c for the DES candidates in Fig. 16. From the top panel of Fig. 16, we see that the greatest mass points are attained for the higher values of ρ_c when the value of m progressively increases from 1 to 2.5. In addition, we find that the maximum mass progressively increases with the increasing value of m.

For our present model, for $m = 1$, 1.5, 2, and 2.5 the maximum masses are obtained as 1.21 $M_\odot$, 1.68 $M_\odot$, 2.05 $M_\odot$, and 2.36 $M_\odot$ respectively and those masses are achieved for $\rho_c = 7.3 \times 10^{14}$ g cm^{-3}, $\rho_c = 1.27 \times 10^{15}$ g cm^{-3}, $\rho_c = 2.02 \times 10^{15}$ g cm^{-3}, and $\rho_c = 2.35 \times 10^{14}$ g cm^{-3} respectively. The Maximum masses have been marked with black dots on the curve.

Figure 16 (right panel) also indicates that the total radius R gradually increases with the increasing value of m. From

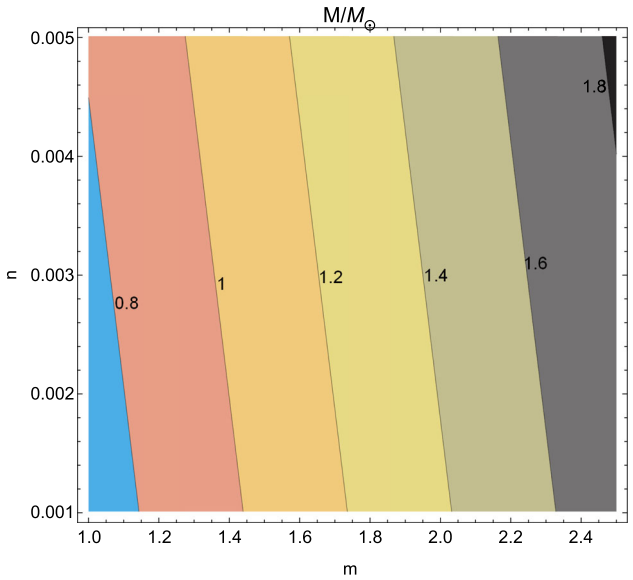

Fig. 15 Contour plot of the mass M($M_\odot$) on $m-n$ plane with $\alpha = 0.25$

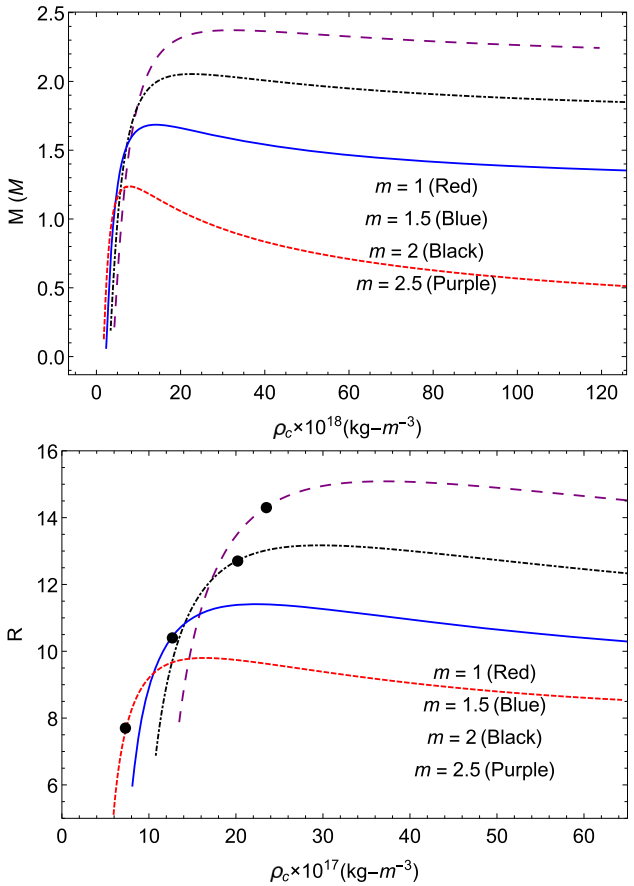

Fig. 16 (Top) M-ρ_c relationship and (bottom) R-ρ_c relationship are shown

this figure, the radius corresponding to the maximum mass points are obtained as 7.7 km, 10.4 km, 12.7 km, and 14.3 km, respectively corresponding to $m = 1,\ 1.5,\ 2$, and 2.5. So, for the increasing value of m, the star becomes large in size and also becomes more massive.

In the context of the metric formalism of $f(R)$ theories of gravity, where R is the Ricci scalar, Pretel and Duarte [103] investigated the hydrostatic equilibrium structure of CSs with the inclusion of anisotropic pressure. They considered the form of $f(R)$ as $f(R) = R^{1+\epsilon}$, where $|\epsilon| \ll 1$. By analyzing the variation of mass with respect to the central density, the authors show that the maximum mass increases with respect to the central density as β increases, where β measures the degree of anisotropy inside the star and in principle can assume positive or negative values. A similar type of result was also obtained by Pretel [102] when they obtained the model of DESs in Einstein's gravity. Tangphati et al. [50] examined that within $f(R, T)$ gravity the maximum mass of the model increases with the increasing value of the coupling constant λ associated with the modified gravity when the Bag constant is fixed. We can compare our findings to the works listed above.

6 Discussion and conclusion

Following Jimenez et al. [52], we proposed a model of a DES in $f(Q)$ gravity in the current work. The model was generated by selecting a linear function with a simplified form of $f(Q)$ given as $f(Q) = mQ + n$, where Q is the non-metricity scalar. Due to the presence of DE, we have assumed that the matter component is made up of two types of fluid: the first is normal baryonic matter, and the second is due to the presence of DE. As a result, the energy–momentum tensor is believed to contain both regular matter and matter related to DE. The goal of the current research is to investigate the stability and physical characteristics of a model of DESs within the context of $f(Q)$ gravity.

The field equations have been solved by considering that the radial pressure connected to DE (p_r^D) is proportional to the density of DE (ρ^D) and the density connected to DE (ρ^D) is proportional to the density of normal baryonic matter (ρ). Her X-1 was taken into consideration as a representative of the stellar candidates in order to highlight various attributes and outcomes of the solutions for the selected parametric values of m. We have chosen four different values of m as $m = 1,\ 1.5,\ 2$, and 2.5. We have calculated the values of different physical parameters presented in metric coefficients for different CS candidates in Table 1. The variation of mass, compactification factor, and redshift with radial coordinates are depicted in Fig. 8. Table 2 shows that the redshift of Her X-1 lies within the range of (0.18, 0.93), for the selected values of m. The values of M/R for all values of m are found in Table. 2 to be well within the Buchdahl limit, i.e.,

Table 1 The numerical values of a, b and d for some familiar compact objects have been obtained

Star	Observed mass ($M_\odot$)	Observed radius (km)	Estimated mass ($M_\odot$)	Estimated radius (km)	a (km^{-2})	b (km^{-2})	d
Her X-1 [71]	0.85 ± 0.15	8.1 ± 0.41	0.85	8.5	0.00483817	0.00289578	−0.558777
SMC X-4 [72]	1.29 ± 0.05	8.831 ± 0.09	1.29	8.8	0.00731424	0.00491954	−0.947383
Vela X-1 [72]	1.77 ± 0.08	9.56 ± 0.08	1.77	9.5	0.00883866	0.00676124	−1.40789
4U 1538-52 [72]	0.87 ± 0.07	7.866 ± 0.21	0.87	7.8	0.0065589	0.00403023	−0.644243
LMC X-4 [72]	1.04 ± 0.09	8.301 ± 0.2	1.04	8.3	0.00669853	0.004256	−0.754658
4U 1608 - 52 [73]	1.74 ± 0.14	9.528 ± 0.15	1.7	9.5	0.00831638	0.00619486	−1.30964

Table 2 The numerical values of central density, surface density, central pressure, α, $u(R)$ and $z_s(R)$ for the CS Her X-1 [71] for different values of 'm'

m	ρ_c (g/cm^3)	ρ_s (g/cm^3)	p_c (dyne/cm^2)	α	$u(R)$	$z_s(R)$
1	7.43111×10^{14}	5.8546×10^{14}	7.85951×10^{34}	0.229256	0.144481	0.185915
1.5	1.13034×10^{15}	8.78189×10^{14}	1.03785×10^{35}	0.152837	0.218031	0.331632
2	1.51865×10^{15}	1.17092×10^{15}	1.28007×10^{35}	0.114628	0.291671	0.549208
2.5	1.90744×10^{15}	1.46365×10^{15}	1.51794×10^{35}	0.0917022	0.365351	0.927005

Table 3 The maximum mass and the corresponding radius of different values of m

m	Maximum mass $M(M_\odot)$	Corresponding radius (in km)	Matched with the mass of the CS
1	1.71	6.77	4U 1608-52 [73]
1.5	1.95	7.3	PSR J1614-2230 [90]
2	2.33	8.4	PSR J0952-0607 [77]
2.5	2.57	9.06	GW 190814 [44]

$M/R < 4/9$. Figure 1 illustrates the variation of the metric potentials with respect to the radial coordinate, indicating the lack of any physical or geometric singularities in our system. Figures 2 and 3 illustrates fluctuations in pressure and density with respect to the radial coordinate. It demonstrates how both physical characteristics are maximum at the center of the star and gradually decrease to their lowest values at the surface.

In Table 2, we have predicted the values for several physical characteristics of the stellar candidate Her X-1 based on parametric values of m for the purpose of comparative analysis. The findings in Table 2 strongly reveal that as m increases, the central density (ρ_c), surface density (ρ_s), and central pressure (p_c) also increase. Figures 2 and 3 precisely demonstrate the same behaviors. It is also clear from Table 2 that α decreases as m increases. Figure 4 depicts the matter density, radial pressure, and transverse pressure related to DE. It shows that the matter density is positive inside the interior of the star, while the radial and transverse pressures are all negative inside the boundary. Figure 7 illustrates the energy conditions for all the chosen values of m and our model is consistent with the energy condition. Figure 9 depicts the variation of V^2 with respect to the radial coordinate. It is confirmed that the system is stable since the square of the sound speed V^2 caused by various values of m has a monotonically decreasing nature throughout the stellar configuration and behaves well as it remains within the limit $[0,\ 1]$.

In addition, Fig. 10 shows that for the selected values of m, the adiabatic indices Γ are greater than $4/3$, providing stability of the system against an infinitesimal radial adiabatic perturbation. Further, we have shown the normalized total mass M vs radius R due to various values of m in Fig. 12. We discover that as m is increased, the maximum mass and their radii gradually increase. For instance, at $m = 1$, the maximum mass and corresponding radius were determined to be $1.71 M_\odot$ and 6.77 km, respectively, whereas, at $m = 2.5$, the maximum mass and corresponding radius were determined to be $2.57 M_\odot$ and 9.06 km, respectively. Figures 13, 14, 15 describe the measurement of mass on $\alpha - m$, $\alpha - n$, and $m - n$ planes in details. Figure 16 depicts the variation of normalized total mass $M(M_\odot$ and R with respect to the central density ρ_c of normal baryonic matter. From our analysis, We find that the maximum mass is obtained as 2.36 $M_\odot$ for $\rho_c = 2.35 \times 10^{15}$ gm cm^{-3} at $m = 2.5$, and the minimum mass is obtained as 1.21 $M_\odot$ for $\rho_c = 7.3 \times 10^{14}$ gm cm^{-3} at $m = 1$. Therefore, essentially, one can note that as the

values of m increase from $m = 1$ to $m = 2.5$, the stellar system becomes more massive and larger in size, so the density increases gradually to produce a more dense stellar system.

Since the underlying composition of DE is still unknown, a detailed study of the internal structure of DESs is even now challenging several models for the interior of the star have been presented so far. In the present work, we have determined the maximum mass of the DES based on the study of the $M - R$ diagram. It is notable that Ghezzi [56] used an analysis of the $M - R$ curve and obtained a DES with a mass of 2 $M_\odot$. The author claims that one of the special features of the mass-radius relation for DESs is that an instability gap arises between the two stable bands, whereas this gap does not exist for TOV NSs. The discovery of this unique gap might indicate a significant interaction between DE and matter which could serve as clear evidence for the validity of the model. Interestingly, Bhar [79] proposed a model for a DES made of dark and ordinary matter in the Tolman-Kuchowicz spacetime geometry in the background of Einstein's gravity and obtained a DES having mass 2.5 $M_\odot$ from the $M - R$ diagram. On the other hand, Pretel [102] explored the possible existence of stable DESs by choosing the Chaplygin-like EoS (i.e. $p_r = A\rho - B/\rho$) which predicts maximum-mass values consistent with observational measurements of highly massive pulsars like J1614-2230 [90], J0348+0432 [81], J0740+6620 [89], J2215+5135 [99], and the lower mass of the compact object detected by the GW190814 event [80]. From the analysis, the author shows that the maximum allowable mass and the corresponding radius increase with an increasing value of α, where α is a dimensionless parameter that controls the amount of anisotropy within the stellar fluid.

In this context, we would like to draw attention to a recent article by Tudeshki et al. [51]. The authors argued that massive gravitons alone can increase the maximum mass radius in the isotropic model. The greatest mass of the DES achieved under massive gravity is in the range (2.95–3.5) $M_\odot$, which falls within the mass gap range (2.5–5) $M_\odot$. The obtained result covers the observational constraints and thus can be a representative of a massive unseen companion in the binary system 2MASS J05215658+4359220, whose mass range is estimated to be $3.3^{+2.8}_{-0.7}$ $M_\odot$ [111] and remnant mass of GW190425 [80,108]. By using a $M-R$ diagram, we are able to relate our recent measurement of the maximum mass of a DES to the earlier researches [51,56,79,102]. We observe that the $f(Q)$ theory can increase maximum masses, allowing DESs to avert gravitational collapse with more mass. This suggests that the theory is capable of explaining the data of massive CSs, such as PSR J1614-2230, PSR J0952-0607, and the lighter component of GW 190814. In the work of Pretel and Duarte [76], the maximum mass of neutron star is obtained as ~ 2 $M_\odot$ with radius about 11 km. In Ref. [104], the authors obtained a neutron star of mass 2 $M_\odot$ with radius $R = 12.12^{+1.11}_{-1.23}$ km. In the work of Bauswein et al. [105], it has been examined that the total mass of GW170817 provides a reliable constraint on the stellar radius if the merger did not result in a prompt collapse as suggested by the interpretation of associated electromagnetic emission. By analyzing a combined dataset from X-ray telescopes NICER and XMM-Newton, Raaijmakers et al. [106] studied the additional impact on the EOS from the jointly estimated mass and radius of PSR J0740+6620. By employing two different high-density EOS parameterizations: a piecewise-polytropic (PP) model and a model based on the speed of sound in a neutron star (CS), the NICER mass-radius estimate of PSR J0030+0451, the authors find the radius of a 1.4 $M_\odot$ neutron star to be constrained to the 95% credible ranges $12.33^{+0.76}_{-0.81}$ km (PP model) and $12.18^{+0.56}_{-0.79}$ km (CS model). In our present model of dark energy stars, we have shown that for small values of the coupling parameter 'm' associated with $f(Q)$ gravity, the dark energy stars (DESs) have mass < 2 $M_\odot$ but for higher values of 'm', the masses of DESs lie in the mass-gap region. From our investigation, it can be also observed that the radii of the DESs are in the range 7–9 km. So DESs are found to be more massive.

Recently, Romano [107] described the impact of DE on GW propagation. Therefore, it may be anticipated that GW astronomy and future electromagnetic investigations of compact binaries would assist in acquiring a better understanding of CSs in the presence of DE. We would like to point out a DES suggested by Rahaman et al. [41] where they have demonstrated that in their model the anisotropic matter is contained within 8 km from the center of the star whereas the outer region comprises a thick shell that extends up to 7 km. Although the thick shell does not exert any radial pressure, it is characterized by zero energy density and non-zero transverse pressure. Hopefully, further observational evidence will support this type of theoretical model.

Finally, as a concluding remark, we would like to point out that DES plays an essential role in the context of $f(Q)$ gravity because the function of the coupling parameter in this gravity makes the proposed model closer to the observational results.

Acknowledgements PB and SR thank the Inter-University Centre for Astronomy and Astrophysics (IUCAA), Pune, Government of India for providing visiting associateship. AE thanks the National Research Foundation (NRF) of South Africa for the award of a postdoctoral fellowship. SR also acknowledges the facility availed under ICARD at CCASS, GLA University, Mathura.

Data availability There are no associated data with this article as such no new data were generated or analyzed in support of this research.

Funded by SCOAP[3]. SCOAP[3] supports the goals of the International Year of Basic Sciences for Sustainable Development.

References

1. F. Bajardi, D. Vernieri, S. Capozziello, Eur. Phys. J. Plus **135**, 912 (2020)
2. S. Mandal, A. Parida, P.K. Sahoo, Universe **8**, 240 (2022)
3. F.K. Anagnostopoulos, S. Basilakos, E.N. Saridakis, Phys. Lett. B **822**, 136634 (2021)
4. R. Solanki, S.K.J. Pacif, A. Parida, P.K. Sahoo, Phys. Dark Univ. **32**, 100820 (2021)
5. U.K. Sharma, Shweta, A.K. Mishra, Int. J. Geom. Methods Mod. Phys. **19**, 2250019 (2022)
6. G. Mustafa, S.K. Maurya, S. Ray, Fortschr. Phys. **2023**, 2200129 (2023)
7. M.K. Jasim, S.K. Maurya, A.K. Jassim, G. Mustafa, R. Nag, I. Saif Al Buwaiqi, Phys. Scr. **98**, 045305 (2023)
8. S.K. Maurya, G. Mustafa, M. Govender, K.N. Singh, JCAP **10**, 003 (2022)
9. P. Bhar, Fortschrit. Phys. 2300074. https://doi.org/10.1002/prop.202300074
10. P. Bhar, J.M.Z. Pretel, Phys. Dark Univ. 101322 (2023)
11. P. Bhar, S. Pradhan, A. Malik, P.K. Sahoo, Eur. Phys. J. C **83**, 646 (2023)
12. P. Bhar, Eur. Phys. J. C **83**, 737 (2023)
13. S.K. Maurya, K.N. Singh, M. Govender, G. Mustafa, S. Ray, Astrophys. J. Suppl. Ser. **269**, 35 (2023)
14. A. de la Cruz-Dombriz, D. Saez-Gomez, Entropy **14**, 1717 (2012)
15. K.V. Staykov, D.D. Doneva, S.S. Yazadjiev, K.D. Kokkotas, JCAP **10**, 006 (2014)
16. S.S. Yazadjiev, D.D. Doneva, K.D. Kokkotas, K.V. Staykov, JCAP **06**, 003 (2014)
17. D.D. Doneva, S.S. Yazadjiev, K.D. Kokkotas, Phys. Rev. D **92**, 064015 (2015)
18. S.S. Yazadjiev, D.D. Doneva, K.D. Kokkotas, Phys. Rev. D **91**, 084018 (2015)
19. S. Capozziello, M. De Laurentis, R. Farinelli, S.D. Odintsov, Phys. Rev. D **93**, 023501 (2016)
20. S.S. Yazadjiev, D.D. Doneva, K.D. Kokkotas, Phys. Rev. D **96**, 064002 (2017)
21. D.D. Doneva, S.S. Yazadjiev, N. Stergioulas, K.D. Kokkotas, Phys. Rev. D **98**, 104039 (2018)
22. S.S. Yazadjiev, D.D. Doneva, K.D. Kokkotas, Eur. Phys. J. C **78**, 818 (2018)
23. G.J. Olmo, D. Rubiera-Garcia, A. Wojnar, Phys. Rep. **876**, 1 (2020)
24. P. Feola, X.J. Forteza, S. Capozziello, R. Cianci, S. Vignolo, Phys. Rev. D **101**, 044037 (2020)
25. V.K. Oikonomou, Symmetry **14**, 1 (2022)
26. A.V. Astashenok, S.D. Odintsov, V.K. Oikonomou, Symmetry **15**, 1141 (2023)
27. V.K. Oikonomou, Mon. Not. R. Astron. Soc. **520**, 2934 (2023)
28. S.D. Odintsov, V.K. Oikonomou, Phys. Rev. D **107**, 104039 (2023)
29. F. D'Ambrosio, S.D.B. Fell, L. Heisenberg, S. Kuhn, Phys. Rev. D **105**, 024042 (2022)
30. A. Kar, S. Sadhukhan, U. Debnath, Mod. Phys. Lett. A **37**, 2250183 (2022)
31. P. Sahoo, A. De, T.H. Loo, P.K. Sahoo, Commun. Theor. Phys. **74**, 125402 (2022)
32. S. Mandal, G. Mustafa, Z. Hassan, P.K. Sahoo, Phys. Dark Univ. **35**, 100934 (2022)
33. A. Errehymy, A. Ditta, G. Mustafa, S.K. Maurya, A.H. Abdel-Aty, Eur. Phys. J. Plus **137**, 1311 (2022)
34. G.N. Gadbail, S. Mandal, P.K. Sahoo, Phys. Lett. B **835**, 137509 (2022)
35. M. Koussour, S. Arora, D.J. Gagoi, M. Bennai, P.K. Sahoo, Nucl. Phys. B **990**, 116158 (2023)
36. G. Chapline, Proceedings of the Texas Conference on Relativistic Astrophysics, Stanford (2004). arXiv:astro-ph/0503200
37. F.S.N. Lobo, Class. Quantum Gravity **23**, 1525 (2006)
38. K.P. Das, U. Debnath, S. Ray, Fortschr. Phys. 2200148 (2023)
39. A.B. Tudeshki, G.H. Bordbar, B.E. Panah, Phys. Lett. B **835**, 137523 (2022)
40. R. Chan, M.F.A. da Silva, J.F.V. da Rocha, Gen. Relativ. Gravit. **41**, 1835 (2009)
41. F. Rahaman, R. Maulick, A.K. Yadav, S. Ray, R. Sharma, Gen. Relativ. Gravit. **44**, 107 (2012)
42. S.S. Yazadjiev, Phys. Rev. D **83**, 127501 (2011)
43. S. Smerechynskyi, M. Tsizh, B. Novosyadlyj, JCAP **02**, 045 (2021)
44. R. Abbott et al. [LIGO Scientific and Virgo], Astrophys. J. Lett. **896**, L44 (2020)
45. C. Ye, M. Fishbach, Astrophys. J. **937**, 73 (2022)
46. F.J. Fattoyev, C.J. Horowitz, J. Piekarewicz, B. Reed, Phys. Rev. C **102**, 065805 (2020)
47. I. Bombaci, A. Drago, D. Logoteta, G. Pagliara, I. Vidaña, Phys. Rev. Lett. **126**, 162702 (2021)
48. G.A. Carvalho, R.V. Lobato, P.H.R.S. Moraes, D. Deb, M. Malheiro, Eur. Phys. J. C **82**, 1096 (2022)
49. D. Deb, F. Rahaman, S. Ray, B.K. Guha, JCAP **03**, 044 (2018)
50. T. Tangphati, I. Karar, A. Pradhan, A. Banerjee, Eur. Phys. J. C **82**, 57 (2022)
51. A.B. Tudeshki, G.H. Bordbar, B.E. Panah, arXiv:2303.04813 [gr-qc]
52. J.B. Jiménez, L. Heisenberg, T. Koivisto, Phys. Rev. D **98**, 044048 (2018)
53. R.H. Lin, X.H. Zhai, Phys. Rev. D **103**, 124001 (2021) [Erratum: Phys. Rev. D **106**, 069902 (2022)]
54. F. Rahaman, S. Ray, S. Islam, Astrophys. Space Sci. **346**, 245 (2013)
55. P.K.F. Kuhfittig, Fund. J. Mod. Phys. **19**, 149 (2023)
56. C.R. Ghezzi, Astrophys. Space Sci. **333**, 437 (2011)
57. K.D. Krori, J. Barua, J. Phys. A Math. Gen. **8**, 508 (1975)
58. M. Kalam et al., Eur. Phys. J. C **72**, 2248 (2012)
59. F. Rahaman, R. Sharma, S. Ray, R. Maulick, I. Karar, Eur. Phys. J. C **72**, 2071 (2012)
60. M. Kalam, F. Rahaman, S.M. Hossein, S. Ray, Eur. Phys. J. C **73**, 2409 (2013)
61. G. Abbas, S. Nazeer, M.A. Meraj, Astrophys. Space Sci. **354**, 449 (2014)
62. G. Abbas, A. Kanwal, M. Zubair, Astrophys. Space Sci. **357**, 109 (2015)
63. G. Abbas, S. Qaisar, M.A. Meraj, Astrophys. Space Sci. **357**, 156 (2015)
64. P. Bhar, Astrophys. Space Sci. **356**, 309 (2015)
65. P. Bhar, Astrophys. Space Sci. **357**, 46 (2015)
66. S. Biswas, S. Ghosh, S. Ray, F. Rahaman, B.K. Guha, Ann. Phys. **401**, 1 (2019)
67. P. Bhar, Eur. Phys. J. Plus **135**, 757 (2020)

68. S. Biswas, D. Deb, S. Ray, B.K. Guha, Ann. Phys. **428**, 168429 (2021)
69. K. Schwarzschild, Sitz. Deut. Akad. Wiss. Math. Phys. (Berlin) **23**, 189 (1916)
70. K. Lake, Phys. Rev. D **67**, 104015 (2003)
71. M.K. Abubekerov, E.A. Antokhina, A.M. Cherepashchuk, V.V. Shimanskii, Astron. Rep. **52**, 379 (2008)
72. M.L. Rawls, J.A. Orosz, J.E. McClintock, M.A.P. Torres, C.D. Bailyn, M.M. Buxton, Astrophys. J. **730**, 25 (2011)
73. T. Guver, F. Özel, A. Cabrera-Lavers, P. Wroblewski, Astrophys. J. **712**, 964 (2010)
74. Y.B. Zeldóvich, I.D. Novikov, *Relativistic Astrophysics. Stars and Relativity*, vol. 1 (University of Chicago Press, Chicago, 1971)
75. O. Sokoliuk, S. Pradhan, P.K. Sahoo, A. Baransky, Eur. Phys. J. Plus **137**, 1077 (2022)
76. J.M.Z. Pretel, S.B. Duarte, Class. Quantum Gravity **39**, 155003 (2022)
77. R.W. Romani, D. Kandel, A.V. Filippenko, T.G. Brink, W. Zheng, Astrophys. J. Lett. **934**, L17 (2022)
78. C.W. Misner, D.H. Sharp, Phys. Rev. **136**, B571 (1964)
79. P. Bhar, Phys. Dark Univ. **34**, 100879 (2021)
80. B.P. Abbott et al. [LIGO Scientific and Virgo], Astrophys. J. Lett. **892**, L3 (2020)
81. J. Antoniadis et al., Science **340**, 1233232 (2013)
82. C.D. Bailyn, R.K. Jain, P. Coppi, J.A. Orosz, Astrophys. J. **499**, 367 (1998)
83. C.G. Bassa et al., Astrophys. J. Lett. **846**, L20 (2017)
84. A.V. Astashenok, S. Capozziello, S.D. Odintsov, V.K. Oikonomou, Phys. Lett. B **816**, 136222 (2021)
85. C.G. Böhmer, T. Harko, Class. Quantum Gravity **23**, 6479 (2006)
86. I. Bombaci, Astron. Astrophys. **305**, 871 (1996)
87. M. Cahill, G. McVittie, J. Math. Phys. **11**, 1382 (1970)
88. S. Chandrasekhar, Astrophys. J. **140**, 417 (1964) [Erratum: Astrophys. J. **140**, 1342 (1964)]
89. H.T. Cromartie et al. [NANOGrav.], Nat. Astron. **4**, 72 (2019)
90. P. Demorest, T. Pennucci, S. Ransom, M. Roberts, J. Hessels, Nature **467**, 1081 (2010)
91. D.D. Doneva, S.S. Yazadjiev, Phys. Rev. D **85**, 124023 (2012)
92. W.M. Farr, N. Sravan, A. Cantrell, L. Kreidberg, C.D. Bailyn, I. Mandel, V. Kalogera, Astrophys. J. **741**, 103 (2011)
93. P.C.C. Freire, S.M. Ransom, S. Begin, I.H. Stairs, J.W.T. Hessels, L.H. Frey, F. Camilo, Astrophys. J. **675**, 670 (2008)
94. N.K. Glendenning, *CSs: Nuclear Physics, Particle Physics, and General Relativity*, 2nd edn. (Springer, New York, 2000)
95. H. Heintzmann, W. Hillebrandt, Astron. Astrophys. **38**, 51 (1975)
96. W. Hillebrandt, K.O. Steinmetz, Astron. Astrophys. **53**, 283 (1976)
97. D. Horvat, S. Ilijic, A. Marunovic, Class. Quantum Gravity **28**, 025009 (2011)
98. B.V. Ivanov, Phys. Rev. D **65**, 104001 (2002)
99. M. Linares, T. Shahbaz, J. Casares, Astrophys. J. **859**, 54 (2018)
100. F. Özel, D. Psaltis, R. Narayan, A.S. Villarreal, Astrophys. J. **757**, 55 (2012)
101. F. Özel, D. Psaltis, R. Narayan, J.E. McClintock, Astrophys. J. **725**, 1918 (2010)
102. J.M.Z. Pretel, Eur. Phys. J. C **83**, 26 (2023)
103. J.M.Z. Pretel, S.B. Duarte, Class. Quantum Gravity **39**, 155003 (2022)
104. S. Altiparmak, C. Ecker, L. Rezzolla, Astrophys. J. Lett. **939**, L34 (2022)
105. A. Bauswein, O. Just, H.T. Janka, N. Stergioulas, Astrophys. J. Lett. **850**, L34 (2017)
106. G. Raaijmakers, S.K. Greif, K. Hebeler, T. Hinderer, S. Nissanke, A. Schwenk, T.E. Riley, A.L. Watts, J.M. Lattimer, W.C.G. Ho, Astrophys. J. Lett. **918**, L29 (2021)
107. A.E. Romano, arXiv:2211.05760 [gr-qc]
108. J. Sedaghat et al., Phys. Lett. B **833**, 137388 (2022)
109. H.O. Silva, C.F.B. Macedo, E. Berti, L.C.B. Crispino, Class. Quantum Gravity **32**, 145008 (2015)
110. L.B. Szabados, Living Rev. Relativ. **7**, 4 (2004)
111. T.A. Thompson et al., Science **366**, 637 (2019)